Reconciling different approaches to quantifying land surface temperature impacts of afforestation using satellite observations

Huanhuan Wang[1], Chao Yue[2,3*], Sebastiaan Luyssaert[4]

[1] ~~-~~College of Natural Resources and Environment, Northwest A&F University, Yangling, Shaanxi 712100, P. R. China

[2] State Key Laboratory of Soil Erosion and Dryland Farming on the Loess Plateau, Northwest A&F University, Yangling, Shaanxi 712100, P. R. China

[3] College of Forestry, Northwest A&F University, Yangling, Shaanxi 712100, P. R. China

[4] Department of Ecological Sciences, Faculty of Sciences, Vrije Universiteit Amsterdam, Amsterdam 1081 HV, The Netherlands

Correspondence: Chao Yue, State Key Laboratory of Soil Erosion and Dryland Farming on the Loess Plateau, Northwest A&F University, Yangling, Shaanxi 712100, P. R. China

E-mail: chaoyue@ms.iswc.ac.cn

Abstract

Satellite observations have been widely used to examine afforestation effects on local surface temperature at large spatial scales. Different approaches, which ~~lead~~ potentially lead to differing~~ed~~ definitions of the afforestation effect, have been used in previous studies. Despite their large differences, ~~The~~ the results of these studies have been ~~were~~ used in climate model validation and ~~were~~ cited in climate synthesis reports~~,~~. ~~but large differences existed in these results.~~ Such differences have been ~~were~~ simply treated as observational uncertainty, which can be an order of magnitude bigger than the signal itself. ~~However, it remains unclear whether these differences arise from methodological differences that can be reconciled or they represent intrinsic uncertainty of land surface temperature change following afforestation.~~ Although the

fraction of the satellite pixel actually afforested has been noted to influence the magnitude of afforestation effect, it remains unknown whether it is a key factor which can reconcile the different approaches. Here, we provide a synthesis of three influential approaches (one estimates the actual effect and the other two the potential effect) ~~used in the literature~~ and use large-scale afforestation over China as a test case to examine whether the different approaches can be reconciled.~~whether the differences in the effects stem from methodological differences.~~ We found that the actual effect (ΔT_a) often relates to incomplete afforestation over a medium resolution satellite pixel (1km). ΔT_a increased with the afforestation fraction, which explained 89% of its variation~~for which LST is observed and that it increases with the fraction of the pixel actually afforested (89% variation in ΔT_a being explained)~~. One potential effect approach quantifies the impact of quasi-full afforestation (ΔT_{p1}), whereas the other quantifies the potential impact of full afforestation (ΔT_{p2}) by assuming a shift from 100% openland to 100% forest coverage. An initial paired-samples *t*-test shows that $\Delta T_a < \Delta T_{p1} < \Delta T_{p2}$ for the cooling effect of afforestation ranging from 0.07K to 1.16K. But when all three methods are normalized for full afforestation, the observed range in surface cooling becomes much smaller (0.79K to 1.16K). ~~While potential cooling effects could indeed be realized through full afforestation, they might not always be feasible, given other environmental constraints such as the high water consumption of forests and competition for land usage. Although potential cooling effects have a value in academic studies where they can be used to establish an envelope of effects, they are misleading in a policy-making context where the actual cooling effect better represents policy ambitions.~~Potential cooling effects have a value in academic studies where they can be used to establish an envelope of effects, but their realization at large scales is challenging given its nature of scale dependency. The reconciliation of the different approaches demonstrated in this study highlights the fact that the afforestation fraction should be accounted for in order to bridge different estimates of surface cooling effects in policy evaluation.

Keywords: surface temperature change, afforestation, actual effect, potential effect, reconciliation, surface energy balance, China

1 Introduction

Afforestation has been and is still proposed as an effective strategy to mitigate climate change because forest ecosystems are able to sequester large amounts of carbon in their biomass and soil, slowing the increase of atmospheric CO_2 concentration (Fang et al., 2014; Pan et al., 2011). Additionally, forests regulate the exchange of energy and water between the land surface and the lower atmosphere through various biophysical effects, including radiative processes such as surface reflectance, and non-radiative processes such as evapotranspiration and sensible heat flux (Bonan, 2008; Juang et al., 2007). As the net result of the surface energy balance, land surface temperature (LST) is widely used to measure the local climatic impact of afforestation (Li et al., 2015; Winckler et al., 2019a).

Climate model simulations and site-level observations have been utilized to explore the impact of forest dynamics on land surface temperature (Lee et al., 2011; Pitman et al., 2009; Swann et al., 2012). However, afforestation impacts on local LST derived from models tend to be highly uncertain as they are limited by the coarse spatial resolution of models and uncertainties in model parameters and processes (Oleson et al., 2013; Pitman et al., 2011), while insights from site-level assessments cannot be extrapolated to large spatial domains (Lee et al., 2011). Alternatively, remote sensing-based LST products enable the assessment of local LST changes due to forest dynamics on large spatial scales (Li et al., 2015; Shen et al., 2020).

A number of studies investigated the surface temperature impact of afforestation based on satellite observations and they have been cited in high-level climate science synthesis reports (e.g., *IPCC Special Report on Climate and Land* authored by Jia et al., 2019), ~~although~~ even though there are large differences in afforestation impacts on LST between~~among~~ different methods. For example, Alkama and Cescatti (2016), found a cooling effect of about 0.02K from afforestation in temperate regions, while Li et al. (2015) reported a 0.27±0.03K ‘potential’ cooling from afforestation in the northern temperate zone (20–50° N) based on the ‘space-for-time’ method. In contrast, Duveiller et al. (2018) found a much stronger ‘potential’ cooling effect of 2.75K for afforestation in the northern temperate region. While such differences were acknowledged in a recent modelling study (Winckler et al., 2019b), they were simply treated as observational uncertainty for climate model evaluation, with the uncertainty range being as big as, or even an order of magnitude larger than, the afforestation effect. It remains unclear whether the differences arising from these different methods can be reconciled.~~However, it remains unclear whether these differences arise from methodological differences that can be reconciled or they indeed represent the intrinsic uncertainty of the afforestation impact on LST.~~

Until now, studies using satellite data to investigate afforestation impact on surface temperature have mainly focused on three methods. The first method, termed the ‘space-and-time’ approach (Fig. 1, red box), aims to examine the actual, realized effect of afforestation (‘actual effect’) by isolating the forest cover change effect from the gross temperature change over time in places where forest cover change actually occurred (Alkama and Cescatti, 2016; Li et al., 2016a). The second method, termed the ‘space-for-time’ approach (Fig. 1, orange box), compares the surface temperature of forest with adjacent ‘openland’ (i.e., cropland or grassland) under similar environmental conditions (e.g., background climate and topography) and estimates the ‘potential effect’ of afforestation if afforestation were to occur (Ge et al., 2019; Li et al., 2015;

Peng et al., 2014). Note that such effects are often quantified using medium-resolution land-cover datasets (typical resolution = 1km), which do not necessarily represent 100% ground coverage, and we therefore term such a potential effect a 'mixed potential effect'.

The third method, recently used by Duveiller et al. (2018), uses the 'singular value decomposition' technique (Fig. 1 green box), which is claimed to extract the hypothetical LST for different land-cover types by assuming a 100% coverage of the target cover type. The afforestation effect on LST is then quantified as the difference between the LST of a pixel with a hypothetical 100% forest coverage and the LST of an adjacent pixel with 100% openland coverage. As with the second method, such an approach quantifies the 'potential effect' of afforestation, but in this case, it quantifies the 'full potential effect' by assuming transitions between land-cover types with 100% complete ground coverage.~~ Given the aforementioned methodological differences and, in particular, the different definitions of afforestation impact on LST, confusion, if not misinterpretation, is expected when LST changes quantified using these different approaches are used for model evaluation or policy recommendation.~~

Previous studies have revealed the fraction of forest change as an important factor determining the magnitude of the afforestation effect. Alkama and Cescatti (2016) indicated that the actual temperature effect is fraction-dependent, and Li et al. (2016a) pointed out that use of a higher threshold to define forest change resulted in a stronger potential effect. Nonetheless, whether the fraction of forest change can explain the differences in the afforestation effect produced by different methods, e.g., whether the 'potential' effect can be 'actualized', has not been demonstrated. Testing the role of afforestation fraction in reconciling the afforestation effects produced by different methods can help clarify potential confusion and contribute to appropriate policy evaluation.

This study develops detailed conceptual and methodological descriptions for each of the three approaches ~~,~~ and uses large-scale afforestation over China as a case study to compare the three approaches. We tested the following hypotheses: (1) The actual effect on LST increases with the area that has actually been afforested, defined as afforestation intensity (or F_{aff}). (2) The actual effect is smaller than the potential effects. (3) When extending F_{aff} to a hypothetical value of 100%, the actual effect approaches the potential effect. If proven, this third hypothesis implies that the LST impacts from different approaches could be reconciled given the same boundary condition of full afforestation. In that case, we then have a fourth hypothesis (4) stating that changes in underlying biophysical processes including radiation, sensible and latent heat fluxes that drive LST changes should also be reconciled among different methods. To keep the focus on reconciling methodological differences, only changes in the daytime surface temperature were considered in this study. Nevertheless, similar conclusions regarding the different approaches are expected for nighttime surface temperature.

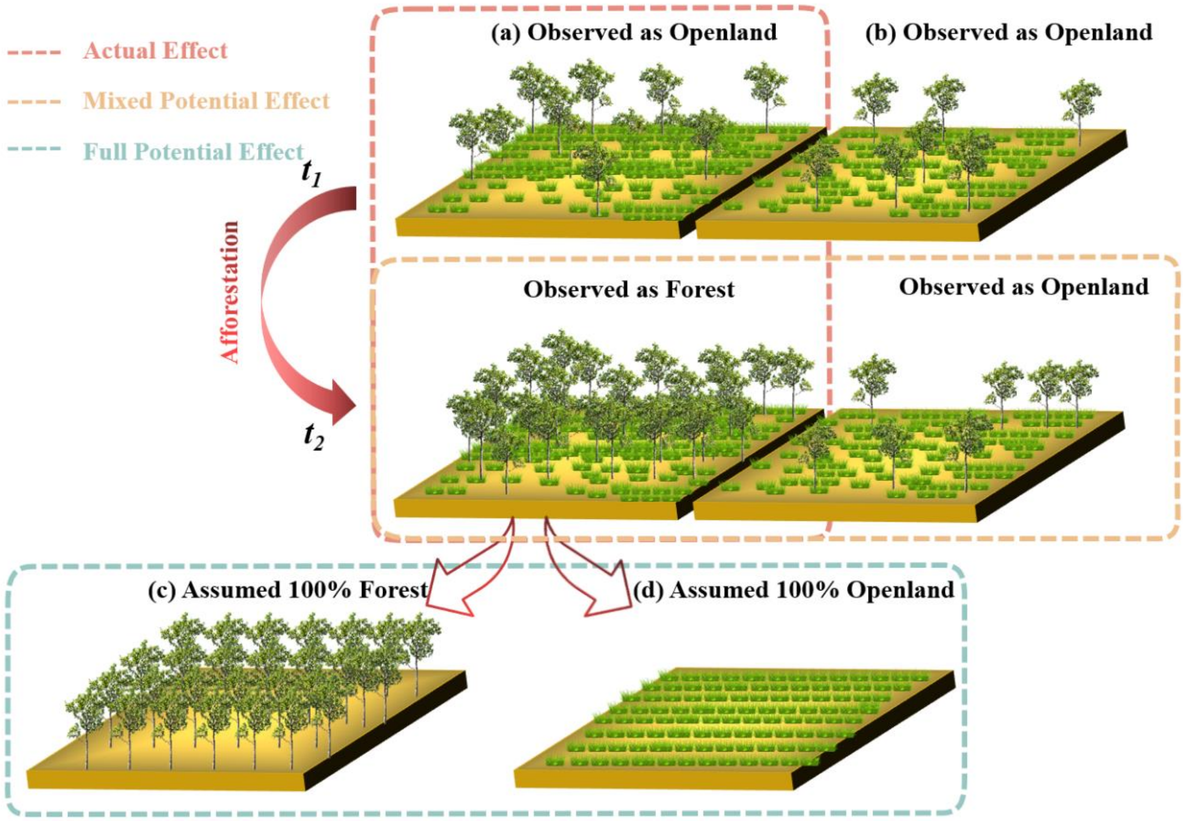

Figure 1. Illustration of the three approaches to quantifying the local surface temperature effect of afforestation. (a) and (b) represent two nearby pixels, both classified as openland at time t_1 by medium-resolution satellites (1km spatial resolution), with one of them classified as forest at time t_2 (i.e., having experienced afforestation) and the other unchanged. Note, neither of these pixels will have 100% complete coverage of either openland (i.e., grassland or cropland) or forest, but they will have been classified as either openland or forest by medium-resolution satellite products. (c) and (d) represent pixels with 100% forest or 100% openland coverage whose temperature can be derived from pixels of mixed land cover types by using the singular value decomposition (SVD) technique (Duveiller et al., 2018). The red dotted box describes the quantification of the 'actual effect' of afforestation (ΔT_a) occurring from t_1 to t_2 by the 'space-and-time' method. The orange box represents the 'mixed potential effect' determined by hypothesizing potential shifts between openland and forest based on the 'space-for-time' approach (ΔT_{p1}). The green box represents the 'full potential effect' of afforestation (ΔT_{p2})

derived by hypothesizing a transition from 100% complete openland coverage to 100% complete forest coverage.

2 Methods

2.1 Three Approaches to Quantifying the Impacts of Afforestation on LST

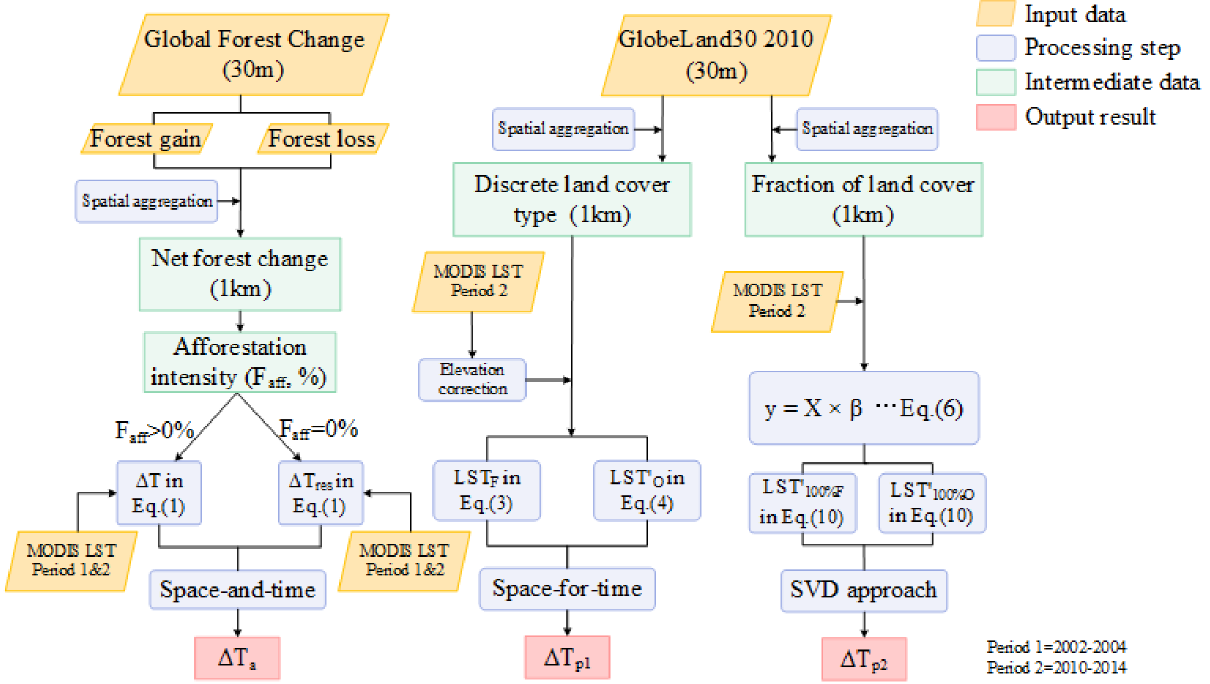

Figure 2. Schematic overview of the processing steps. The different output results correspond to actual effect (ΔT_a), mixed potential effect (ΔT_{p1}) and full potential effect of afforestation (ΔT_{p2}).

2.1.1 Actual Effect of Afforestation (ΔT_a)

The 'space-and-time' approach assumes that the gross change in land surface temperature (ΔT) over a given time period during which afforestation occurred, contains both signals of temperature change due to afforestation (ΔT_a) and background temperature variation (ΔT_{res}) due to changes in large-scale circulation patterns (Alkama and Cescatti, 2016; Li et al., 2016a):

$$\Delta T = \Delta T_a + \Delta T_{res} \quad (1)$$

where ΔT is the gross temperature change during the period from t_1 to t_2 for the pixel under study. ΔT can be calculated as the difference between LST_{t2} and LST_{t1}, with LST_{t2} being the surface temperature after afforestation and LST_{t1} being that before afforestation. It thus follows that

$$\Delta T_a = \Delta T - \Delta T_{res} \quad (2)$$

ΔT_{res} can be approximated by averaging changes in surface temperature for those pixels adjacent to the target afforestation pixel for which the forest cover remained constant between t_1 and t_2 (i.e., F_{aff} =0%; section 2.2.2). Here, pixels with F_{aff} > 0% were defined as afforestation target pixels. A searching window of 11 km by 11 km was established, centered on the afforestation pixel. Within this window, pixels with F_{aff} =0% were defined as control pixels and were used to derive ΔT_{res}. ~~Here, a search window of 11 km×11 km centered on the afforestation target pixel was used to derive ΔT_{res}.~~ Afforestation pixels and adjacent control pixels were both determined based on the net forest change between t_1 and t_2 using Global Forest Change (GFC) data (Fig. 2; ~~section~~ Section 2.2.2).

2.1.2 Mixed Potential Effect (ΔT_{p1})

The ‘space-for-time’ method relies on the ‘space-substitute-for-time’ assumption to obtain the potential impact of afforestation on local temperature (Zhao and Jackson, 2014). By assuming that forest and openland share the same environmental conditions (background climate, topography, etc.) within a small spatial domain, the potential temperature effect of afforestation is examined using the search window method with a window size of up to 40km×40km (Ge et al., 2019; Li et al., 2015; Peng et al., 2014). Here, to be consistent with our ‘actual effect’ approach, a more conservative window size of 11km×11km was used, smaller than that used in the majority of previous studies (Ge et al., 2019; Li et al., 2015; Peng et al., 2014). In most previous studies, existing medium resolution (1km) land-cover maps were used directly. Such land-cover products rely on certain thresholds to classify satellite pixels into discrete land-cover types. Given the widespread spatial heterogeneity in land-cover distribution, it is to be expected that only in rare cases will these medium-resolution pixels have 100% coverage of a given land-cover type. Therefore, when determined in this way, the potential effect of afforestation has been named the 'mixed potential effect', in contrast to the 'full potential effect', on which we will focus in the next section, –which assumes a potential transition between land-cover types of 100% coverage~~ that we will focus on in the next section. ~~.

To ensure consistency with the land-cover data used in the 'full potential effect' approach (i.e., the SVD method), the GlobeLand30 land-cover map was aggregated from its original resolution (30m) to 1km resolution. The land-cover type assigned to a given 1km pixel during aggregation was based on the land-cover type with an area fraction >50% within that pixel,~~The land-cover type assigned to a given 1km pixel during aggregation was based on the land-cover type of the majority of the 30m sub-pixels within the 1km pixel,~~ to be consistent with the~~ ideas~~ rationale behind the generation of medium-resolution land-cover products (~~section ~~Section 2.2.2). A 1km forest pixel was then chosen as the target pixel and put at the center of a search window with dimensions 11km×11km. The 'mixed potential effect' of afforestation (ΔT_{p1}) was defined as the difference between the temperature of the target pixel (LST_F) and the average temperature of all the surrounding openland pixels within the window ($\overline{LST_O'}$):

$$\Delta T_{p1} = LST_F - \overline{LST_O'} \quad (3)$$

where LST_F is the surface temperature of the target forest pixel at t_2, and LST_O' represents the elevation-corrected surface temperature of openland pixels at t_2 within the search window. Given our search window size, ΔT_{p1} could be biased by the elevation difference between the target forest pixel and surrounding openland pixels. Therefore, a linear relationship was first fitted between the observed openland temperature, LST_O, and the elevation of the openland pixel (Ele_O). This fitted temperature lapse rate was then used to derive elevation-corrected openland temperature LST_O':

$$LST_O' = LST_O + k \times \Delta Ele_{F\text{-}O} \quad (4)$$

where $\Delta Ele_{F\text{-}O}$ is the elevation difference between forest and openland pixels. The elevation is available from NASA's Shuttle Radar Topography Mission (SRTM) data (https://lpdaac.usgs.gov/products/srtmgl1v003/).

2.1.3 Full Potential Effect (ΔT_{p2})

The full potential effect represents the temperature change due to hypothesizing a shift from 100% openland to 100% forest coverage, and was determined here by employing the singular value decomposition (SVD) method used in Duveiller et al. (2018). The SVD technique assumes that the temperature observed for a pixel at 1km scale is a linear composition of the temperatures of different land-cover types at a finer resolution (in our study at a 30m resolution). For each 1km pixel, the observed temperature ~~at 1km resolution~~ can be written as the composition of the temperature of each component land-cover type and its corresponding fraction, based on the land-cover fractions derived from the 30m-resolution GlobeLand30 map (~~section~~ Section 2.2). The temperature of each type of land cover was assumed constant within a search window of 11km × 11km. For each given search window, the following equations can be obtained:

$$\begin{pmatrix} y_1 \\ \vdots \\ y_n \end{pmatrix} = \begin{pmatrix} x_{11} & \cdots & x_{1m} \\ \vdots & \ddots & \vdots \\ x_{n1} & \cdots & x_{nm} \end{pmatrix} \times \begin{pmatrix} \beta_1 \\ \vdots \\ \beta_m \end{pmatrix} \quad (5)$$

where n is the total number of 1km pixels within the window, after accounting for the elevation difference (thus the maximum value of n is 121 given our 11km × 11km search window), m is the number of land-cover types, x_{ij} refers to the fraction of land-cover type *j* in pixel *i*, β_i refers to the temperature of land cover type *i*. To minimize elevation impacts, the linear regression relationship for a given 1km pixel was included only when the elevation difference between this pixel and the central pixel of the search window was smaller than 100m. Using matrix notation, Eq. (5) can be simplified to:

$$y = X \times \beta \tag{6}$$

where the matrix X contains land-cover fraction for the *n* 1km pixels as an explanatory variable, the response variable y contains *n* LST observations, and the coefficient vector, β, contains the regression coefficients which show temperatures of different land-cover types. Note that this linear equation system cannot be ~~readily~~ easily solved ~~simply~~ because the matrix X is 'closed', i.e., by definition, the elements in each row of the matrix X add to 1. After removing the mean of each column (Zhang et al., 2007), the matrix X was transformed, by applying the SVD technique, to another matrix, Z, of reduced dimension (more details in Duveiller et al., 2018). After this transformation, we have the following:

$$y = Z \times \beta^{'} + \varepsilon \tag{7}$$

~~and~~ in which the β' coefficient can be obtained from equation (8):

$$\beta^{'} = \left(Z^{t}Z\right)^{-1} Z^{t}y \tag{8}$$

However, the β' vector calculated from the transformed matrix Z cannot directly provide surface temperatures for corresponding land-cover types. To obtain temperatures for each land-cover type by assuming 100% ground coverage, an identity matrix Y with its dimension equal to the number of land-cover types must be constructed to represent the hypothetical case in which each 1km pixel was 100% covered by a single land-cover type. The same transformation as applied to the matrix X was then applied to Y, to obtain a transformed matrix Z'. Finally, the predicted temperature ($LST'_{100\%}$) for each land-cover type assuming a 100% coverage ~~was~~ is calculated as:

$$LST'_{100\%} = Z' \beta' \tag{9}$$

For the central pixel of the local search window, ΔT_{p2} ~~was~~ is defined as the difference between the predicted $LST'_{100\%}$ for forest ($LST'_{100\%F}$) and openland ($LST'_{100\%O}$).

$$\Delta T_{p2} = LST'_{100\%F} - LST'_{100\%O} \tag{10}$$

More details, including an illustration of the SVD method, can be found in Fig. 7 in Duveiller et al. (2018).

At the scale of the searching windows used in this analysis (11km×11km), any nonlocal effects cancel out when comparing temperature differences over neighboring areas because the effects of advection and atmospheric circulation have been reported to be similar for adjacent areas (Pongratz et al., 2021; Winckler et al., 2019a). Hence the quantified afforestation effect for each of the three methods can be considered to be the local effect only.

2.2 Dataset and Processing

2.2.1 The Test Case: Large-scale Afforestation over China

China was selected as the test case for addressing the important methodological issues in quantifying land surface impacts of afforestation because afforestation is a key national strategy for sustainable development and climate mitigation (Bryan et al., 2018; Qi et al., 2013). According to the 8th National Forest Inventory conducted in 2013, China~~'~~’s afforestation area has reached 6.9×10^3 million ha, accounting for 33% of the total global afforestation area (Chen et al., 2019). Afforestation in China during 2000–2012 occurred mainly in regions with more than 400 mm of precipitation per year (Fig. 3a), which is considered a threshold below which there is a high risk of afforestation failing due to water limitation (Mátyás et al., 2013). China covers a wide range of latitude from 3.9° N to 53.6° N and its forest ecosystems cover an elevation range of 100m to 4000m. This wide range of climate zones, from tropical/subtropical to temperate and boreal, make it highly suitable for our methodological analysis because the impact of afforestation on LST might differ with latitude and background climate (Lee et al., 2011; Alkama and Cescatti, 2016). Further justification for using China as a test case ~~are the~~ comes from the strongly diverging published LST impacts of afforestation there, which range~~ing~~ from an actual effect of -0.0036K decade^{-1} by Li et al. (2020) to a potential effect of -1.1K by Peng et al. (2014).

2.2.2 MODIS Dataset and Preparation

In this study, the actual effect was estimated by combining the actual satellite-derived afforestation for 2000 to 2012 (see Section 2.2.2) with satellite-based estimates of biophysical variables for the periods 2002–2004 (t_1) and 2010–2014 (t_2). MODIS remote sensing products for land surface temperature (MOD11A2), albedo (MCD43B3) and evapotranspiration (MOD16A2) were used to characterize the biophysical effects (Table 1). The datasets were regridded to harmonize with spatial (1km) and temporal (annual) resolutions (Table 1).

The MOD11A2 product provides 8-day land surface temperature for 10:30 AM and 22:30 PM from the Terra satellite, but here we focused on daytime surface temperature. Only valid LST observations from the original data were used to compute the average daily values for a given year. Years for which more than 40% of daily data are missing were excluded from the analysis.

Annual data were then aggregated to obtain the average annual temperature for periods t_1 and t_2.

The MCD43B3 product provides white-sky and black-sky shortwave albedo at 16-day temporal resolution (Table1). The observed white-sky albedo was used as the daytime albedo (Peng et al., 2014). For evapotranspiration (ET), we used the ET band in MOD16A2, which includes water fluxes from soil evaporation, wet canopy evaporation and plant transpiration. To calculate the mean annual albedo and evapotranspiration for 2002–2004 (t_1) and 2010–2014 (t_2) we used the same approach as used for LST.

2.2.3 Land-Cover Datasets and Processing

Two land-cover datasets were used in this study: the 'actual effect' approach was based on the Global Forest Change (GFC) dataset, while the 'mixed potential effect' and 'full potential effect' used the GlobeLand30 land-cover data (Table 1).

The SVD technique, used in the 'full potential effect' approach, requires a land-cover map with a higher spatial resolution than the 1km spatial resolution of the LST data. The GlobeLand30 product, which is based on Landsat images, provides land-cover information for China at a 30m resolution for the years 2000 and 2010 (Chen et al., 2015). Cultivated land and grassland in GlobeLand30 were classified as openland. Discrete land-cover type information at 30m resolution in 2010 was aggregated to obtain the area fractions of the different land-cover types at 1km resolution, which were then used to construct matrix X in Eq. (5) (Fig. 2). Furthermore, land-cover type information at the 1km scale was extracted, based on the vegetation type with area fraction >50% for every 1km×1km window. This data was then applied in the 'space-for-time' method to identify forest and openland (Fig. 2).

GlobeLand30 data is not suitable for detecting forest change (Zeng et al., 2021). The Global Forest Change (GFC) data, however, provides forest gain and forest loss at a spatial resolution of 30m between 2000 and 2012 and has been used for mapping global forest change (Hansen et al., 2013). This product shows an overall accuracy of greater than 99% for areas of forest gain at the global scale when compared with statistical data reported in Forest Resource Assessment (FRA), LiDAR detection (Geoscience Laser Altimetry System), and MODIS NDVI time series (Hansen et al., 2013), and thus has been recommended for use in forest and forest-change estimates (Chen et al., 2020; Zeng et al., 2021). Using this dataset, ~~F~~forest loss events were identified for each year between 2000 and 2012, but forest gain was only identified for the whole period, simply because forest loss is an abrupt change which can be effectively identified over short time periods, ~~but~~ whereas forest gain is a gradual change which can only be confidently identified over longer time spans. Here, forest losses and gains from GFC were aggregated at a 1km resolution to obtain net forest change (defined as forest gain minus forest loss) during this period (Fig. 2). A positive net change indicates afforestation and the area percentage of afforestation for the 1km pixel area was defined as F_{aff}. The land-cover type of pixels with F_{aff} = 0% was considered to be stable. This net forest-change information was then used in the calculation of the actual afforestation-induced temperature effect (ΔT_a)(Fig. 2).

2.3 Decomposition of Changes in Surface Temperature

Changes in surface temperature following forest-cover change are the net result of changes in underlying fluxes that collectively determine the land surface energy balance:

$$\Delta SW_{in} - \Delta SW_{out} + \Delta LW_{in} - \Delta LW_{out} = \Delta H + \Delta LE + \Delta G \quad (11)$$

where ΔSW_{in}, ΔSW_{out}, ΔLW_{in}, ΔLW_{out} are the changes in incoming and outgoing shortwave and longwave radiation, respectively, and ΔH, ΔLE, and ΔG are changes in sensible heat flux, latent heat flux and ground heat flux, respectively. All the terms of Eq. (11) are expressed in Wm^{-2}.

Firstly, it can be reasonably assumed that $\Delta SW_{in} \approx 0$ and $\Delta LW_{in} \approx 0$, given that all three approaches consider only local effects on surface temperature by following a comparison of target pixels with surrounding control pixels, thus excluding feedbacks from, e.g., cloud formation (Duveiller et al., 2018). Changes in reflected shortwave radiation can be derived as:

$$\Delta SW_{out} = SW_{in} \times \Delta\alpha \quad (12)$$

where SW_{in} is available from the CERES EBAF-Surface Product Ed 4.1 (Kato et al., 2018; Liu et al., 2018) (Table 1), and Δα is the surface albedo change. To approximate ΔLW_{out}, we used its first order differential equation:

$$\Delta LW_{out} = \sigma(4\varepsilon_B T^3 \Delta T + \Delta\varepsilon_B T^4) \quad (13)$$

where σ is Stefan-Boltzmann's constant (5.67×10^{-8} W m^{-2} K^{-4}), T is daytime surface temperature and ΔT is the afforestation impact on surface temperature. Surface broadband emissivity, ε_B, is usually obtained from an empirical relationship (Zhang et al., 2019):

$$\varepsilon_B = 0.2122\varepsilon_{29} + 0.3859\varepsilon_{31} + 0.4029\varepsilon_{32} \quad (14)$$

where ε_{29}, ε_{31} and ε_{32} are obtained from the estimated emissivity for bands 29 (8,400–8,700 nm), 31 (10,780–11,280 nm) and 32 (11,770–12,270 nm) in the MOD11C3 data (Duveiller et al., 2018).

Latent heat flux change (ΔLE) refers to changes in the energy used for evapotranspiration (ET, unit: mm d^{-1}), which can be obtained from the change in evapotranspiration (ΔET):

$$\Delta LE = \Delta ET \times 28.94\ \mathrm{W\ m^{-2}/(mm\ d^{-1})} \tag{15}$$

Therefore, the sum of sensible heat change and ground heat change ($\Delta H+\Delta G$) can be calculated as the difference between net radiation change and latent heat flux change (ΔLE) based on ~~the~~ Eq. (11). The afforestation effects on albedo ($\Delta\alpha$), ε_B ($\Delta\varepsilon_B$) and ET (ΔET) needed in the above equations were calculated in a similar way to ΔT for each of the three different approaches as described in ~~section~~ Section 2.1.

2.4 Statistical Analysis

The spatial distributions of original samples for the three methods are different because of the different land-cover maps used (Fig. 2 and Figure A1) and, therefore, the statistical analysis was limited to those pixels shared by all three approaches: 96,058 sample pixels at 1km resolution. The distribution of these shared sample pixels retained the characteristics of the spatial distribution of the original samples (Figure A2).

Differences in the afforestation effects on LST of the three approaches were tested by performing paired-samples *t*-tests between pairs of approaches. The paired-samples *t*-test was used, rather than a normal *t*-test, to avoid the bias due to strong spatial heterogeneity in the LST effects of afforestation that could occur if the values of all pixels had been pooled together for a normal *t*-test. ~~The pairing in the paired-samples *t*-test limits the analysis to only those pixels shared by all three approaches.~~ The test was made using the ‘ttest_rel’ method from the ‘scipy.stats’ package in Python. The Bonferroni correction was applied to adjust the significance level (p-value) to mitigate the increasing ~~the t~~Type I error when making multiple paired-samples *t*-test, which in our case involves three pairs~~.~~ (Lee and Lee, 2018; UC Berkely, 2008). The Bonferroni correction sets the significance cut-off at α/k (with α as the p-value before correction and k as number of pairs). In this study, with 3 hypotheses tests (i.e., 3 pairs) and an original significance level α = 0.05, the adjusted p-value is 0.0167. In order to investigate ΔT_a in relation to the afforestation intensity, a linear regression was performed between ΔT_a and F_{aff} using the ordinary least squares method.

Table 1 Summary of the datasets and their main characteristics

Type	Dataset	Selected band	Resolution	Projection	Timespan
Forest change	Global Forest Change	Forest gain; Loss year	30m, annual	WGS84	2000–2012
Land-cover type	GlobeLand 30	Land-cover type	30m, —	UTM	2000; 2010
Land surface Temperature	MOD11A2	Daytime temperature	1km, 8days	sinusoidal	2002–2004; 2010–2014
Albedo	MCD43B3	Albedo WSA shortwave	1km, 16days	sinusoidal	2002–2004; 2010–2014
Incoming shortwave radiation	CERES	sfc_sw_down _all_mon	1°, monthly	WGS84	2002–2004; 2010–2014
Surface broadband emissivity	MOD11C3	Emis_29; Emis_31; Emis_32	0.05°, monthly	sinusoidal	2002–2004; 2010–2014
Evapotranspiration	MOD16A2	ET_500m	500m, 8days	sinusoidal	2002–2004; 2010–2014

Elevation	SRTM30	Be75	30m, —	WGS84	—

3 Results

3.1 Spatial Distribution of Afforestation and its Effect on Land Surface Temperature

In China, ~~A~~afforestation areas are mainly located in the northeast, southwest and south~~ of China~~, where sufficient precipitation is available (Fig. 3a) and largely driven by afforestation of former cropland or abandoned cropland, with a relatively small contribution from forest regeneration or replanting following natural disturbance or timber harvest. One prominent feature of afforestation in China is its small afforestation patch, with most afforested pixels ($1km^2$) having an afforestation fraction of less than 30% (Fig. 3b). Pixels with an afforestation intensity below 10% account for 93% of the total number of pixels (Fig. 3b), representing 0.14 Mha,~~ or over~~ more than half (55.6%) of the total afforestation area (Fig. 3b).

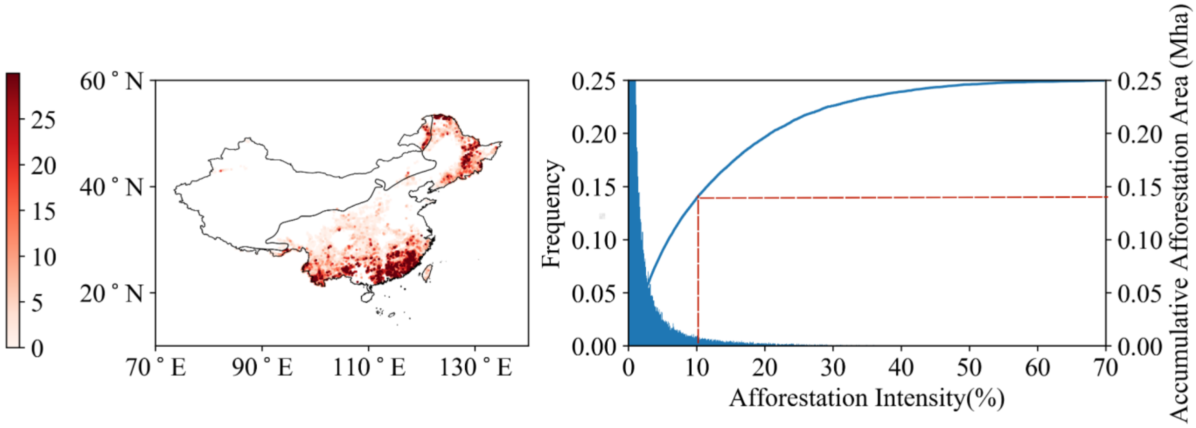

Figure 3. (a) Spatial distribution of afforestation intensity (F_{aff}) in China during 2000–2012. The solid black line crossing China is the 400mm annual precipitation isoline. (b) Frequency distribution of F_{aff} and cumulative afforestation area with the increase in F_{aff}. The red dashed line represents the cumulative afforestation area corresponding to F_{aff} =10%.

Although all three approaches result in similar spatial and latitudinal patterns regarding afforestation effects on LST (Fig. 4), their magnitudes differ substantially. The actual effect has the lowest temperature change, followed by the mixed potential effect, with the full potential effect showing the greatest temperature change (Fig. 4a–c). For the latitude range of 20–36° N where afforestation effects show a dominant cooling effect, the full potential effect (ΔT_{p2}) reaches -1.75±0.01K, while the mixed potential effect (ΔT_{p1}) was smaller at -0.96±0.00K, but both of them were much larger than the actual effect (ΔT_a) of -0.09±0.00K. Similarly, the full potential effect (ΔT_{p2}) showed the strongest warming effect (0.35±0.01K) in the area north of 48° N, stronger than the mixed potential effect (0.22±0.01K), and again the actual effect is the smallest (0.07±0.01K). However, regarding the latitude where the effects change from a warming to cooling effect, the three approaches largely converge ~~regarding the latitude where the effects change from a warming to cooling effect~~ (Fig. 4d). Between 40° N and 48° N, the afforestation effects are largely neutral, with the mean temperature change for the three approaches being 0.07±0.01K (ΔT_a=-0.01±0.01K; ΔT_{p1}=0.11±0.01K; ΔT_{p2}=0.12±0.01K).

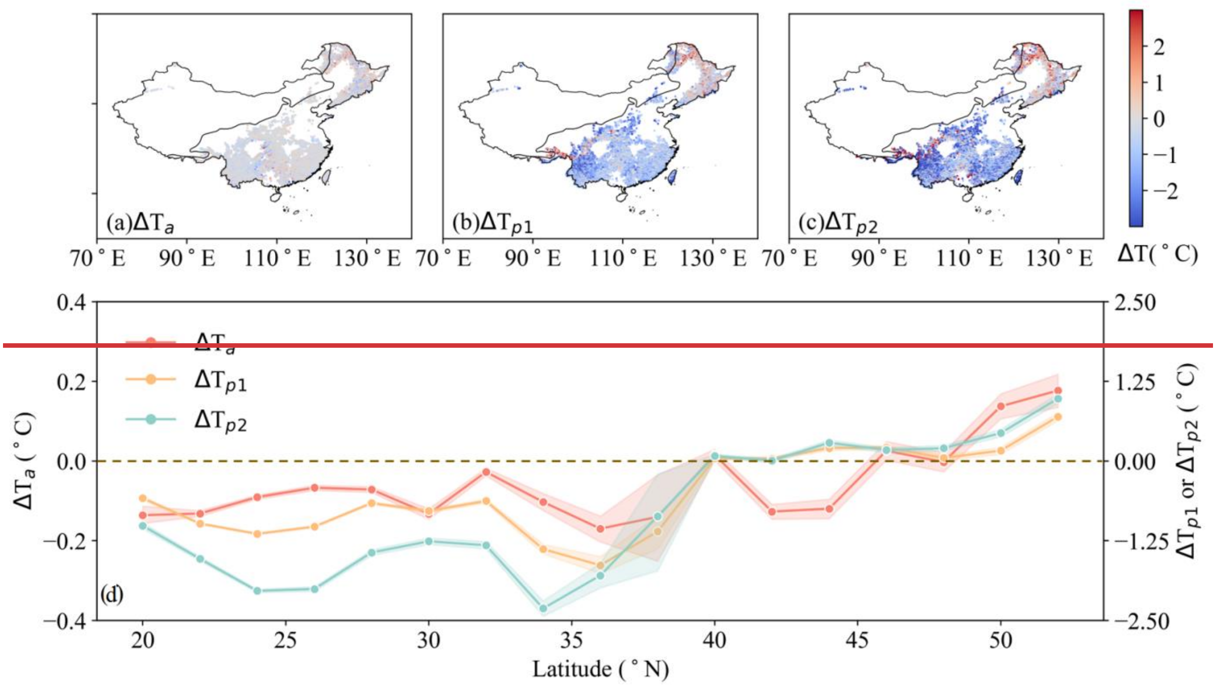

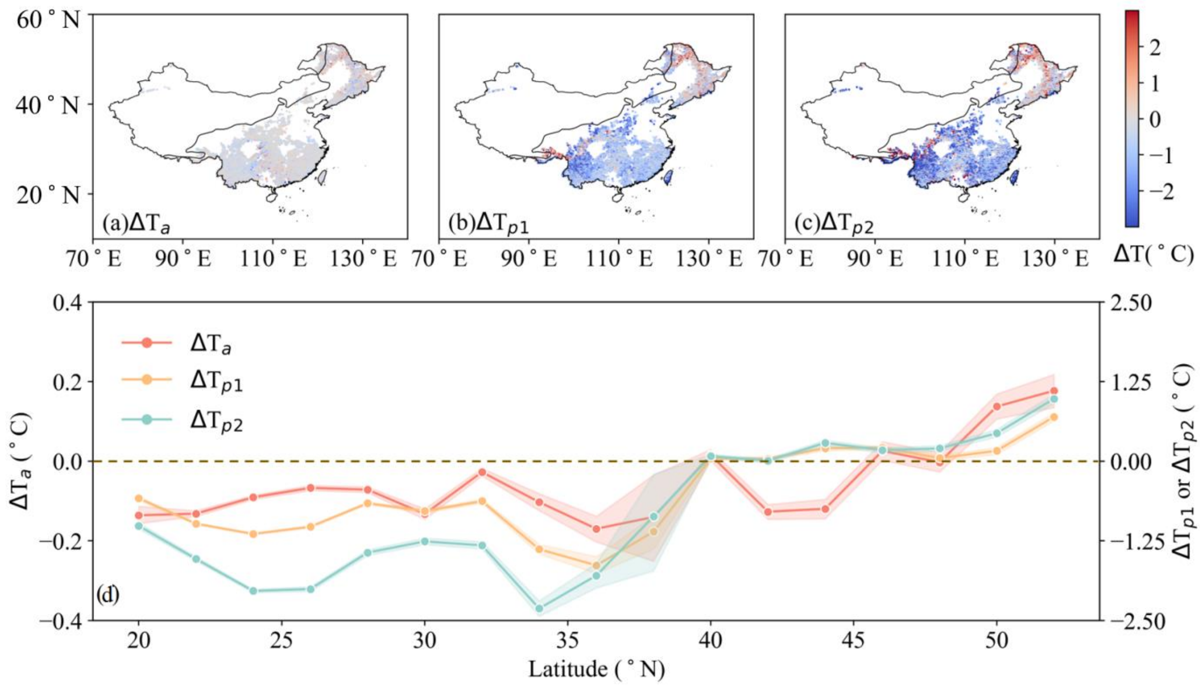

Figure 4. Afforestation effects on LST quantified by three approaches: (a) actual effect based on a 'space-and-time' approach (ΔT_a), (b) mixed potential effect based on a 'space-for-time' approach (ΔT_{p1}) and (c) full potential effect assuming a transition from 100% openland coverage to 100% forest coverage using the SVD method (ΔT_{p2}). The solid black line crossing China is the 400mm precipitation isoline. (d) Zonal averages of the annual mean daytime LST

change within 2° latitudinal bins, with shaded areas representing the standard errors (SE). Note that in panel (d), ΔT_a corresponds to the vertical axis on the left; ΔT_{p1} and ΔT_{p2} correspond to the vertical axis on the right.

3.2 Reconciling Temperature Effects of Afforestation

Even though the observed land surface temperature is assumed to be uniform for the 1km afforested satellite pixel, the underlying afforestation intensity varies substantially (Fig. 3a). This leads to our first hypothesis that for a 1km pixel, ΔT_a should be influenced by the area fraction that has been afforested within the pixel (i.e., afforestation intensity or F_{aff}). Indeed, the actual daytime surface cooling increases significantly with afforestation intensity (Fig. 5), with a 0.079±0.017K (mean ± std) increase for each ten percent increase in F_{aff}.

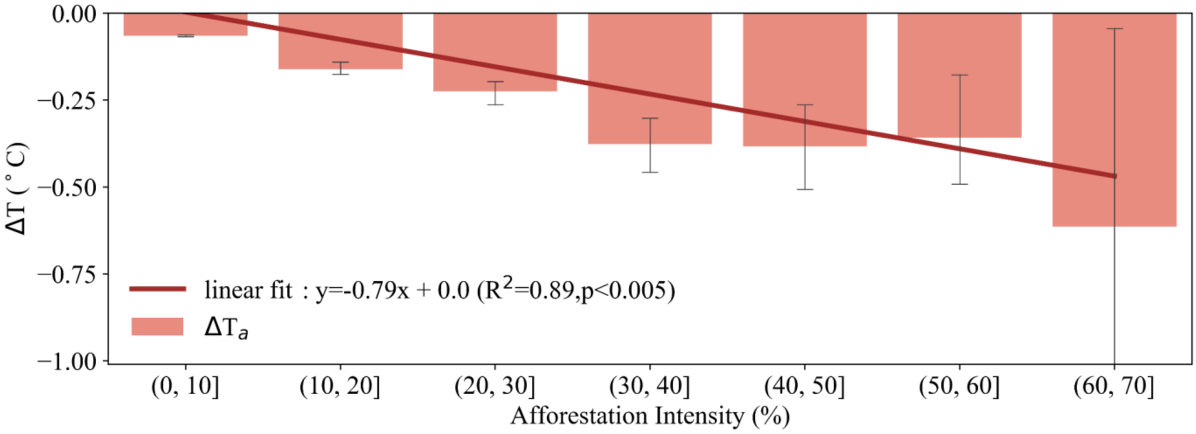

Figure 5. Changes in ΔT_a as a function of afforestation intensity (F_{aff}), defined as the fraction of afforested area to the total pixel area at a 1-km resolution. Error bars indicate the standard error of ΔT_a within each ten percent bin of F_{aff}. The red line represents the fitted linear regression line between ΔT_a and F_{aff}.

The afforestation effects obtained from the three approaches were compared for each F_{aff} interval (Fig. 6). When afforestation intensity is less than 60%, significant differences exist in the temperature change obtained by the three approaches, with $\Delta T_a < \Delta T_{p1} < \Delta T_{p2}$. This result confirms our second hypothesis that the actual effect is expected to be smaller than potential effects. However, for pixels with relatively low F_{aff}, the mixed potential effect is found to be smaller than the full potential effect, which is reasonable, but to our knowledge, has not been reported before. When the afforestation intensity is greater than 60%, the significant difference in cooling effect between the different approaches disappears, likely because afforestation intensity, and the associated forest coverage at 1km resolution, reach ~~high~~ values high enough to allow the 'potential' effects to be realized. ~~, i.e., allowing the 'potential' effects to actually be realized given a high enough afforestation intensity.~~

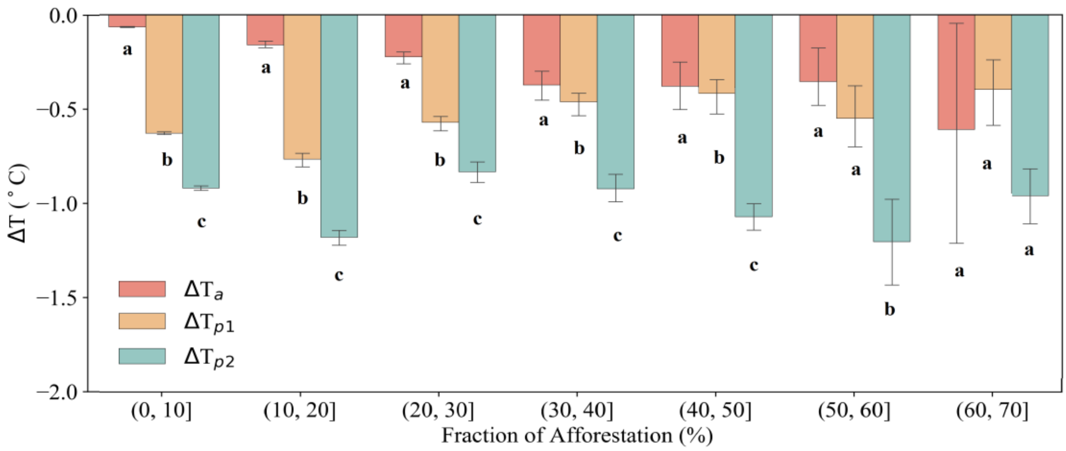

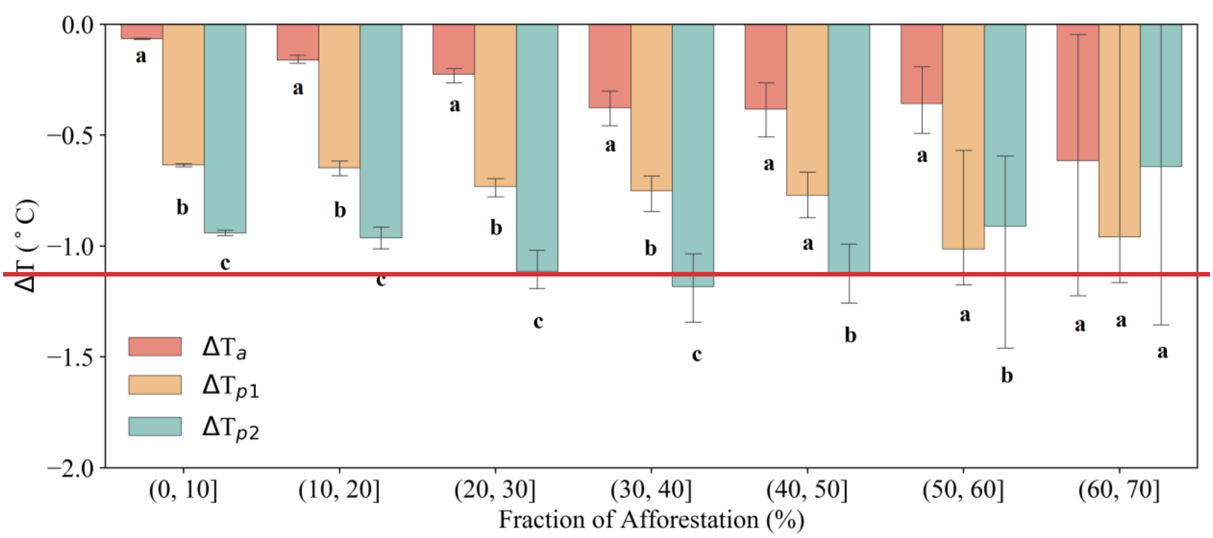

Figure 6. Comparison of ΔT for the three approaches for bins of afforestation intensity. Error bars are given as the standard error and different letters indicate that ΔT calculated by the two approaches concerned are significantly different ~~with~~ using the adjusted p-value after applying the Bonferroni correction ~~with~~ for multiple paired-samples *t*-tests.

When considering the overall differences in ΔT ~~from~~ for the three approaches, irrespective of the afforestation intensity, ΔT_a (-0.07±0.00K) over China was significantly lower than ΔT_{p1} (-0.63±0.00K), which is further significantly lower than ΔT_{p2} (-1.16±0.01K) ($p < 0.05$, paired-samples *t*-test, n= 96,058), once again confirming our second hypothesis (Fig. 7). Moreover, extrapolation of the relationship shown in Fig. 5 suggests that ΔT_a would reach -0.79±0.17K (mean ± std) if a 1km pixel was 100% afforested, which is conceptually comparable to the potential effects. ΔT_a ~~and it~~ was indeed found to be higher than ΔT_{p1} but lower than ΔT_{p2}. This result confirms our third hypothesis and demonstrates that the potential cooling effect could indeed be reached when a pixel is fully afforested.

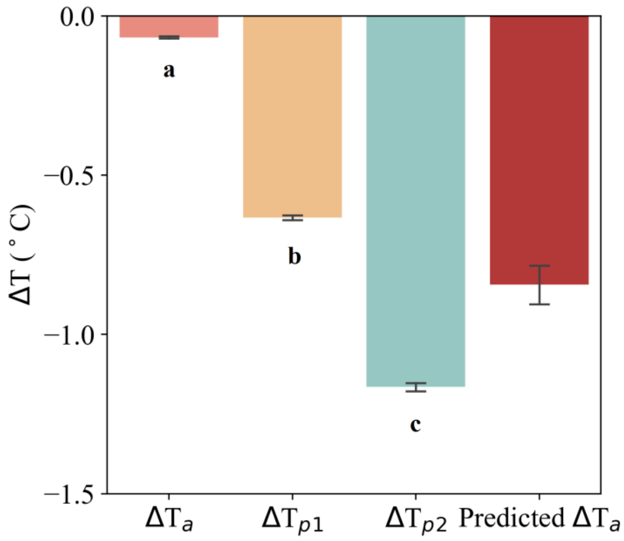

Figure 7. Comparison of ΔT for the three approaches, irrespective of the afforestation intensity. Error bars are given as the standard error and different letters indicate ΔT being significantly different (p = 0.0167, paired-samples *t*-test, n = 96,058). For comparison, the predicted ΔT_a with F_{aff} reaching 100%, which is conceptually comparable with ΔT_{p1} and ΔT_{p2}, is also shown.

3.3 Reconciling Changes in Surface Energy Fluxes by Afforestation

In order to investigate whether the underlying surface energy fluxes could be reconciled following the reconciliation of the LST changes, changes in surface energy fluxes due to afforestation were quantified using each of the three approaches, under the same boundary conditions as for full afforestation (i.e., changes following the 'actual effect' approach were extended for F_{aff} = 100%). As illustrated in Fig. 8, changes in all the relevant surface energy fluxes under the three different approaches have the same direction, with similar magnitudes, confirming the reconciliation of the different approaches in terms of surface energy fluxes. More specifically, the three approaches converge on a reduction in reflected shortwave radiation (ΔSW_{out}) of 0.56~1.23 W m^{-2} due to the lower albedo of forest compared to openland (Figure ~~A2~~A3). ~~Meanwhile, e~~Emitted longwave radiation (ΔLW_{out}) was reduced by 1.03~3.10

W m^{-2} and sensible and ground heat fluxes ($\Delta H+\Delta G$) reduced by 4.84~6.14 W m^{-2}. All these reduced fluxes were offset by an increased latent heat flux of 7.99~8.41 W m^{-2} (ΔLE), the single energy flux leading to surface cooling.

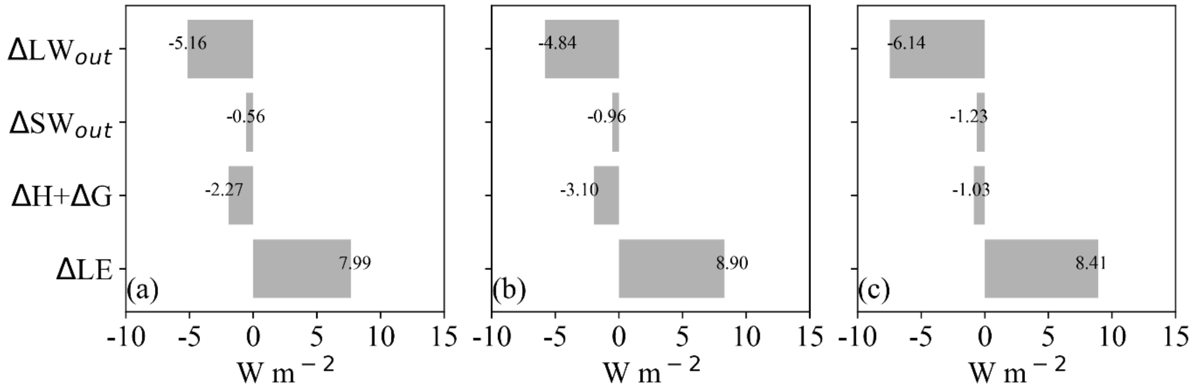

Figure 8. Afforestation-induced changes in surface energy fluxes (Wm^{-2}) following the three approaches: (a) actual effect based on a ‘space-and-time’ approach, (b) mixed potential effect using medium-resolution land cover maps based on a ‘space-for-time’ approach and (c) full potential effect assuming a transition from 100% openland coverage to 100% forest coverage using the SVD method. For each approach, changes were calculated for the reflected shortwave radiation (SW_{out}), outgoing longwave radiation (LW_{out}), latent heat flux (LE) and the combination of sensible and ground heat fluxes (H+G). No changes were assumed for incoming shortwave and longwave radiation. Changes in energy fluxes for the ‘actual effect’ approach have been adjusted to the condition of full afforestation (i.e., F_{aff} = 100%) in a similar way as for the ‘predicted ΔT_a’ in Fig. 7, by fitting linear regressions between energy flux variables and F_{aff} (Figure ~~A1~~A4).

4 Discussion

The three approaches (Li et al., 2015; Alkama and Cescatti, 2016; Duveiller et al., 2018) used to quantify local surface temperature change following forest-cover change and presented with details in this study, have been cited over 919 times in research papers (Web of Science, December 2021) and in high-level climate science synthesis reports. Despite the apparently large differences in temperature effect among them, to our knowledge, no studies have examined whether these differences can be reconciled~~ or whether they represent intrinsic differences~~. This study fills that gap by comparing the three approaches for a single study case, i.e., large-scale afforestation in China. China is highly suitable for the purpose of this study as the size of an afforestation patch is, in general, smaller than the spatial resolution (1km) at which the temperature effects of afforestation were conducted in the previous studies describing the three approaches (Li et al., 2015; Alkama and Cescatti, 2016; Duveiller et al., 2018). Hence, the difference between the actual and potential temperature effects is expected to be large.

Indeed, we found surface cooling following afforestation was much less when estimated as the actual effect (ΔT_a) compared to the potential effects (ΔT_{p1} and ΔT_{p2}). This lower ΔT_a has been attributed to incomplete afforestation at a 1km resolution, at which potential effects are quantified by assuming complete afforestation (i.e., a complete shift from openland to forest). Consistent with our first hypothesis, the afforestation fraction at a 1km resolution explained 89% of the variation in ΔT_a, making it a key determinant of the surface cooling following afforestation (Fig. 5). This result is consistent with the fact that the observed temperature for a mixed surface is determined by the area fractions of its respective components, with each component having a unique temperature. This fact also forms the theoretical foundation for the SVD technique used to derive the full potential effect (Duveiller et al., 2018). ~~This finding is in line with the fundamental fact that surface temperature can be largely treated as an extensive variable: a variable whose whole pixel value of a given property is strongly determined by the area fractions of its different components, with each component having a unique value for the given property. The observation that surface temperature is an extensive variable served as the~~

~~theoretical foundation for the SVD technique to derive the full potential effect (Duveiller et al., 2018).~~

Modelling (Li et al., 2016b) ~~as well as~~and satellite-based (Alkama and Cescatti, 2016) studies have found that temperature change after afforestation (or deforestation) is highly sensitive to the fraction of the model grid cell or satellite pixel that is subjected to afforestation (or deforestation), echoing our finding that ΔT_a significantly changes with F_{aff}. In addition, we provide strong evidence in support of our third hypothesis that when F_{aff} reaches 100%, the expected actual effect is comparable to the potential effects (Fig. 7). This finding shows that the ~~the~~ three approaches compared ~~in this study~~here are consistent when the same boundary condition, i.e., full afforestation, is applied, and demonstrates that all three methods are mutually compatible. It is, therefore, the basis of the reconciliation of the three approaches. ~~Meanwhile, it~~ It also highlights ~~that~~ the fact that the actual afforestation area must be considered when evaluating the climate mitigation effects of afforestation.

Our results also show that the mixed potential effect (ΔT_{p1}) is smaller than the full potential effect (ΔT_{p2}) (Fig. 6, Fig. 7). We suspect that this phenomenon likely also relates to the incomplete forest coverage for the identified forest pixels at the 1km scale used in the 'space-for-time' analysis, because a threshold value of 50% forest cover was used when upscaling the 30m land-cover map to 1km resolution. This threshold, however, is consistent with the commonly applied value in land-cover classification based on medium resolution satellite images, such as MCD12Q1, which uses a tree coverage value of 60% to identify forest pixels (Sulla-Menashe and Friedl, 2018). For the purpose of comparison, we also calculated the mixed potential effect based on the MCD12Q1 land-cover map but using the same LST data. The result shows that potential effects derived using MCD12Q1 data versus those derived using spatially upscaled GlobeLand30 data are almost identical (Figure ~~A3~~A5), lending credibility to our estimated ΔT_{p1} in comparison to previous studies using MODIS land-cover data (Li et al., 2015). Progressively increasing the forest-cover threshold from 50% to 90% steadily increases ΔT_{p1} from -0.62±0.02K to -0.75±0.02K (Figure ~~A4~~A6). Further increasing the thresholds used to identify 1km-resolution openland pixels from 50% to 90% increases ΔT_{p1} from -0.63±0.00K to -1.10±0.02K (Figure ~~A5~~A7), bringing ΔT_{p1} even closer to ΔT_{p2} (-1.16±0.01K). This is consistent with the finding of a previous study on the dependence of the temperature effect on the forest cover change thresholds that were used to define afforestation: the higher the threshold, the stronger the impact on temperature (Li et al., 2016). Our results add ~~This adds~~ further support to the compatibility of the three approaches given the same boundary condition, i.e., the complete transformation from full openland to full forest coverage.

Several factors may contribute to the remaining differences in the temperature effects produced by different methods even after reconciliation. As described in the Method section, there are discrepancies in the assumptions of the three approaches, which lead to differences in the control pixels (i.e., adjacent comparison pixels). For instance, for the ‘pure potential effect’ it is assumed that the LSTs for pixels with the same land cover type are uniform and forest pixels are compared with openland pixels, whereas the in the ‘mixed potential impact’ approach the central target forest pixel is compared with the mean value of non-forest pixels within the searching window. Moreover, space-for-time is an assumption that cannot be verified (Chen et al., 2016), and which will inevitably result in differences in the estimated actual and potential effects, although the consistency between ‘potential’ and ‘actual’ effects after reconciliation in our study does illustrate the broad validity of this assumption.

Differences between the actual and potential temperature effects can also arise from the time period elapsed following afforestation. The temperature effect caused by deforestation is considered to be instant (Liu et al., 2018), while, in contrast, afforestation-driven surface temperature change depends on different stages of forest development and is expected to saturate only when the forest canopy stabilizes (Ziter et al., 2019). The GFC dataset used in this analysis defined forest gain using the condition of successful detection of a stable closed forest canopy that is clearly different from a non-forest state (Hansen et al., 2013), which enhances the chance of temperature change saturation following afforestation. But, given a maximum stand age of 12 years inferred from the GFC dataset, differences in surface temperatures may still exist between newly established forests and the mature existing forests that were used in the ‘potential effect’ approaches. Thus, we cannot exclude the possible contribution of such a mechanism to the difference between the actual and potential effects, which failed to be reconciled.

Previous analyses have documented latitudinal patterns of surface temperature change induced by afforestation (Alkama and Cescatti, 2016; Li et al., 2015, 2016a; Peng et al., 2014). When comparing the three approaches for a single case study, consistent latitudinal patterns of local surface temperature effects following afforestation are observed (Fig. 4). Notably, all three approaches show a warming effect in the northern high latitudes and an opposite cooling effect in the southern low latitudes, with a largely neutral effect in the 40–48° N latitude band, providing further evidence that the three approaches are compatible. In particular, although the three approaches used different land-cover maps, they derived consistent LST impacts following afforestation, which highlights that fact that the reconciliation provided in this study is rather robust and ~~the reconciling provided in this study is rather robust and is~~ unlikely to be dependent on the land cover datasets used.

In addition to the reconciliation of the land surface temperature change, we checked and confirmed that the changes in surface energy fluxes that underlie and drive the changes in surface temperature are compatible under the boundary condition of full afforestation. This finding confirms the inherent consistency in the three approaches and clarifies the reasons behind the apparent discrepancies in existing studies as discussed in the introduction. Nonetheless, when it comes to the biophysical impacts of afforestation in the real world, our findings have far-reaching implications. Full afforestation is often possible at small spatial scales but becomes challenging at large scale. Therefore, the realization of the full potential effect by afforestation is scale-dependent. ~~Although the 'potential effect' of afforestation could indeed be reached, the condition of full afforestation might not be feasible in reality.~~ For example, a complete afforestation of the semi-arid Loess Plateau in the northwest of China is predicted to generate a surface cooling effect of 2.40±0.07K, but substantial afforestation efforts over the past 4 decades in that region have only realized a cooling of 0.11±0.01K as measured by the 'actual effect'. Because of greater water consumption by forest compared to openland and the need to maintain land area for food production, achieving the full cooling potential may not be feasible (Huang et al., 2018; Liu and She, 2012; Liang et al., 2019).

Potential cooling effects have a value in that they can serve to establish the envelope of effects and measure possible outcomes given the condition of full afforestation. However, given the challenge of full afforestation at large spatial scales, potential effects should be converted into a more realistic estimate (i.e., actual effects), by taking into account the intensity of afforestation, to better represent policy ambitions.~~Whereas potential cooling effects have a value in academic studies where they can serve to establish the envelope of effects, they are misleading in a policy-making context where the actual cooling effect better represents policy ambitions.~~ The analog could also be made for the effects of the surface energy impacts of afforestation. Taking 10% as the afforestation intensity threshold to compare the cumulative surface energy effect between the actual and potential approaches, actual cumulative biophysical changes (5.06 EJ) for 2000–2012 are much smaller than mixed potential changes (20.13 EJ) and full potential change (19.02 EJ) (methods in Text A1; Figure A8)~~(Figure A6)~~. Again, this shows that simply using the potential effects for policy making or evaluation risks greatly overestimating the biophysical effects of afforestation.

5 Conclusions

In this study we provided a synthesis of the three influential methods used to quantify afforestation impact on surface temperature change and provided evidence that these different methods could in fact be reconciled. The actual effect of surface temperature change following afforestation was highly dependent on the intensity of afforestation (F_{aff}), which explained 89% of the variation in ΔT_a. With the common boundary condition of full afforestation being applied, differences in afforestation impacts on LST reported by the three methods in previous studies greatly reduced, showing that simply treating these differences as uncertainty is incorrect and could greatly overestimate the uncertainty. In other words, when full afforestation is assumed, the actual effect approaches the potential effect, demonstrating the effectiveness of the 'space-for-time' approach and that the potential cooling effect of afforestation could ~~be~~ indeed be realized. Potential cooling effects have a value in academic studies where they can be used to establish an envelope of effects, but their realization at large scales is challenging given the scale dependency. The reconciliation of the different approaches demonstrated here stresses that the afforestation fraction should be accounted for in order to bridge different estimates of surface cooling effects in policy evaluation.

~~However, due to the environmental constraints such as water availability and land scarcity, large-scale full afforestation might not always be feasible. In this case, potential effect would provide an envelop of the effects of afforestation but only the actual effect has a direct policy relevance in evaluating the climate effects of afforestation projects.~~

Appendix A

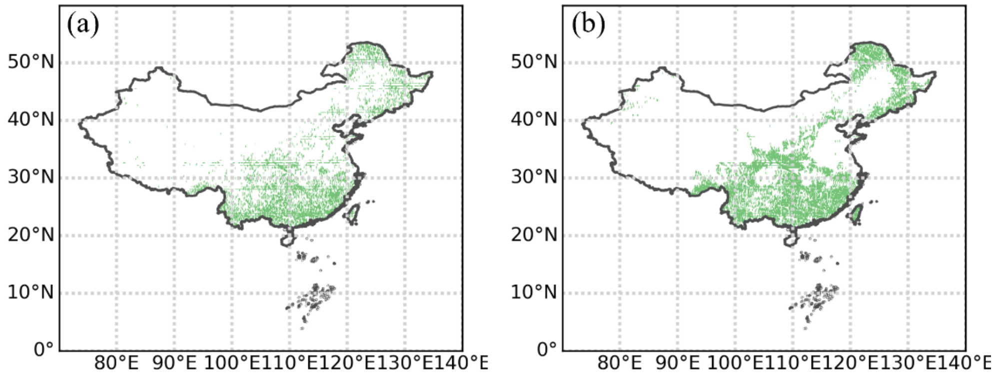

Figure A1. The distributions of the original sample pixels (at a 1km resolution) for (a) the actual effect and (b) the two potential effects.

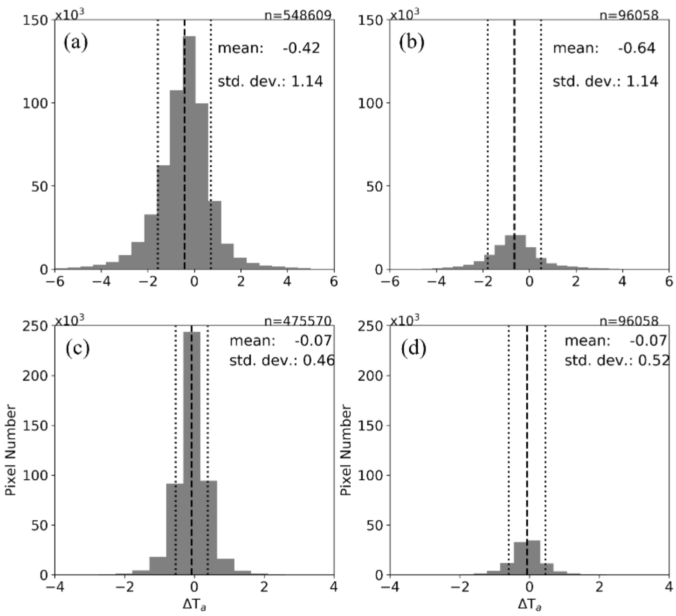

Figure A2. (a) Histogram of ΔT_a of all pixels based on the GFC dataset (b) Histogram of ΔT_a for samples used for the statistical test. (c) Histogram of ΔT_{p1} of all pixels based on GFC dataset (d) Histogram of ΔT_{p2} for samples used for the statistical test.

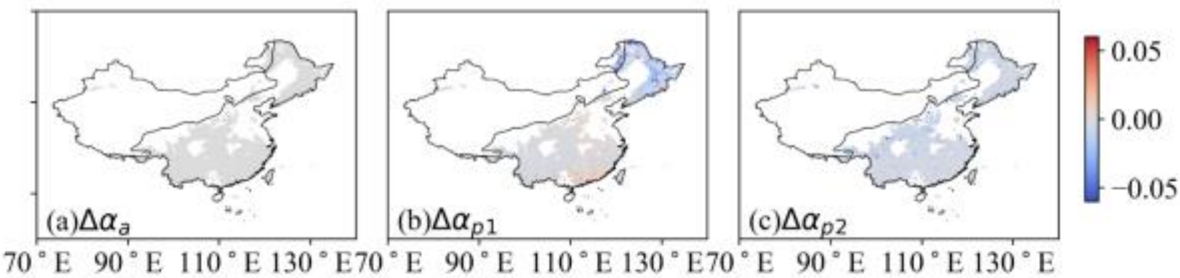

Figure ~~A2~~A3. Spatial distribution of afforestation-induced changes in albedo (α) over China from three approaches: (a) Actual albedo change following afforestation based on 'space-and-time' method ($\Delta\alpha_a$), (b) mixed potential albedo change using medium-resolution land-cover maps based on 'space-for-time' approach ($\Delta\alpha_{p1}$) and (c) full potential effect ($\Delta\alpha_{p2}$) based on SVD approach.

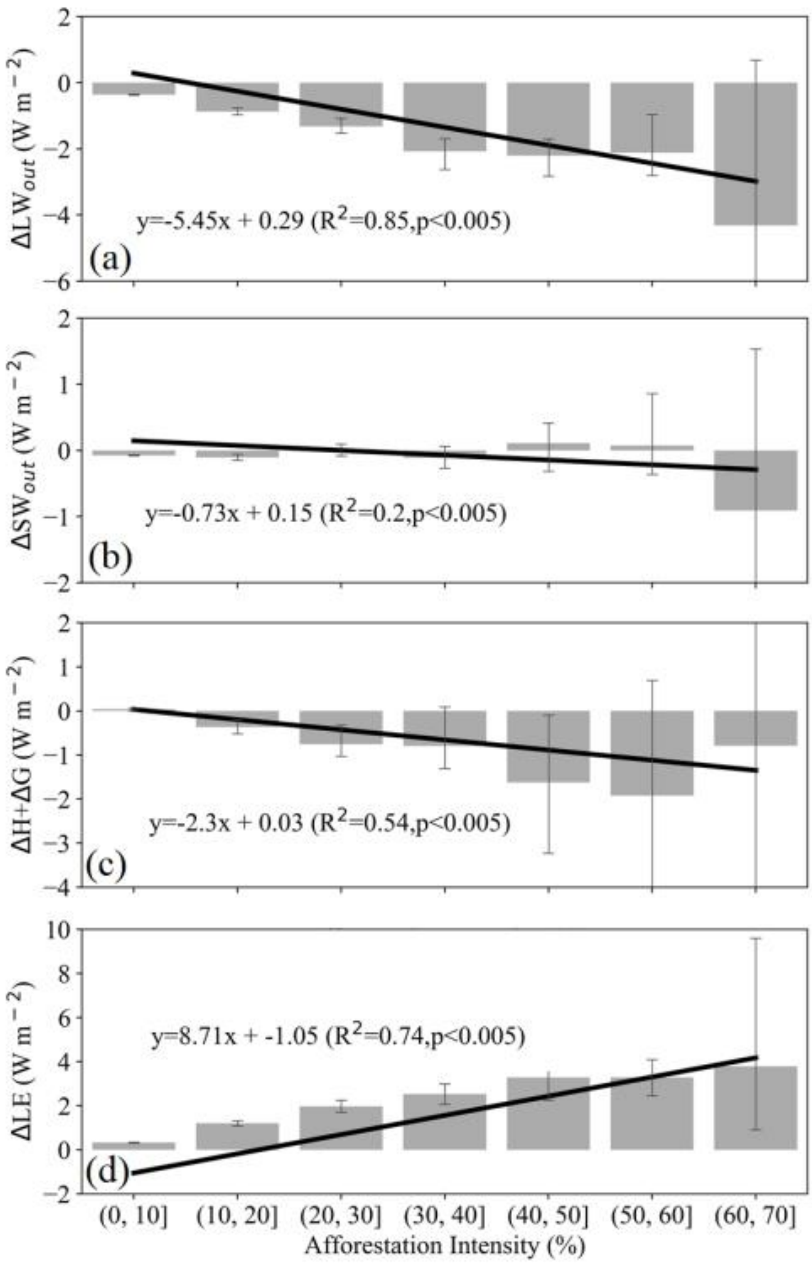

Figure ~~A1~~A4. Changes of actual effect in (a) ΔLW, (b) ΔSW, (c) ΔH+ΔG and (d) ΔLE (W m^{-2}) as a function of afforestation intensity (F_{aff}) following the 'actual effect' approach. Error bars indicate the standard error within each ten percent bin of F_{aff}. The solid black lines represent the fitted linear regression line between each energy flux variable and F_{aff}.

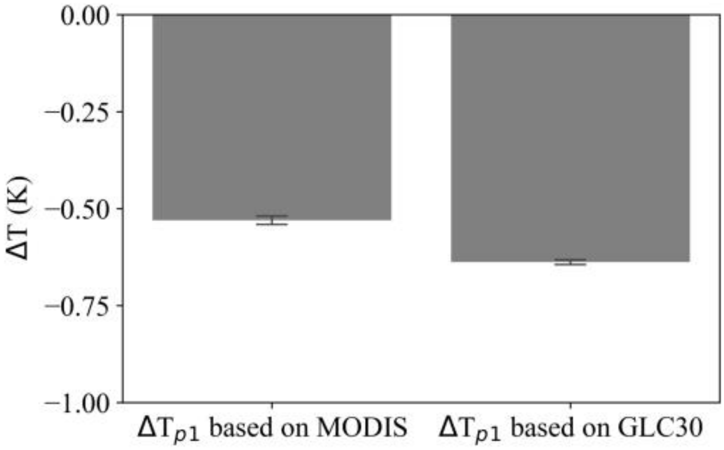

Figure ~~A3~~A5. The mixed potential effects (ΔT_{p1}) obtained based on MODIS land-cover data (MCD12Q1) and the land-cover distribution map defined at the threshold of 50% GlobeLand30 at 1 km resolution.

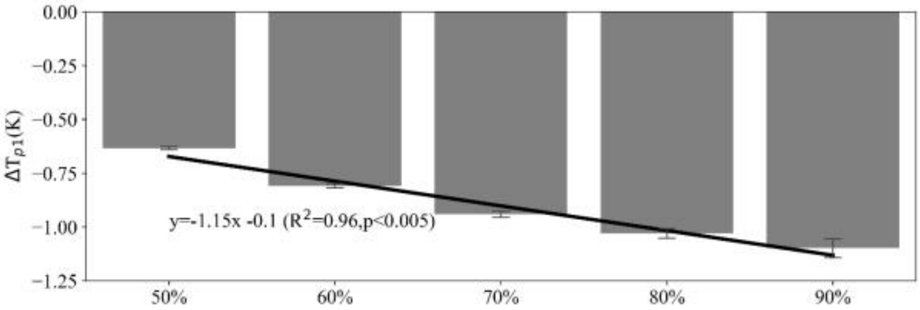

Figure ~~A4~~A6. The influence of the forest-cover threshold applied to the land-cover map underlying the estimation of the mixed potential effect (ΔT_{p1}).

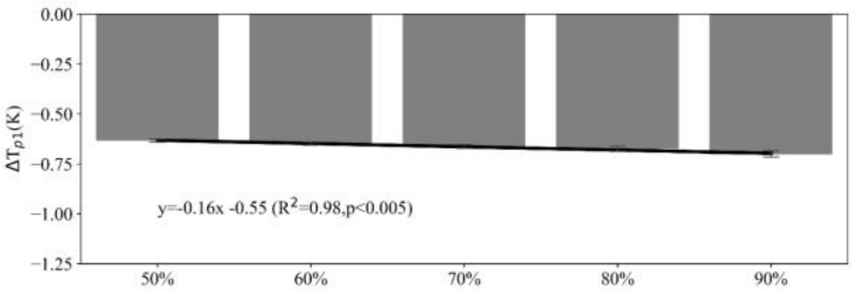

Figure ~~A5~~A7. The influence of the openland-cover threshold used to identify a 1km pixel as openland in the estimation of the mixed potential effect (ΔT_{p1}).

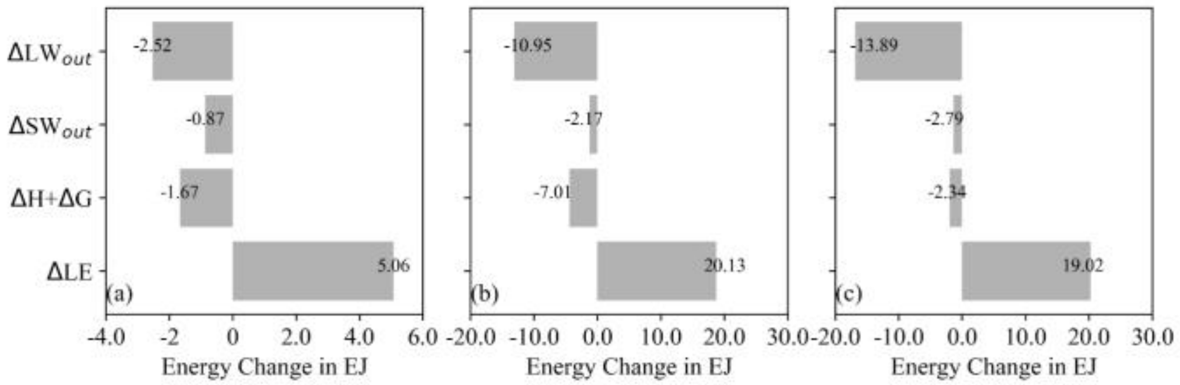

Figure ~~A6~~A8. Afforestation-induced cumulative changes in surface energy fluxes (exaJoules) in China for the period 2000–2012 following the approaches of (a) actual effect, (b) mixed potential effect and (c) full potential effect (methods in Appendix Text A1).

Text A1

The cumulative surface energy effect (f_{cum}) in Figure A8 refers to the sum of the flux change (J) from all the samples, while at the same time accounting for the forest change area (m^2). More specifically, the cumulative surface energy change (f_{cum}) can be calculated from equation A1:

$$f_{cum} = \sum_{i=1}^{i=n}(area_i \times F_i) \qquad \text{(A1)}$$

where F_i is the flux change per unit area ($W\ m^{-2}$) for pixel i, n is the total number of samples, and $area_i$ is the forest change area in pixel i.

–Data availability

All datasets used in this study are summarized in Table 1 and are openly available. Albedo, transpiration and surface temperature data can be accessed at (https://modis.gsfc.nasa.gov/data/). The Global Forest Change data is available from https://earthenginepartners.appspot.com/science-2013-global-forest/. The land-cover type dataset (GlobeLand30) can be downloaded from http://www.globallandcover.com/. Incoming shortwave radiation data can be accessed at https://ceres.larc.nasa.gov/data/. The elevation data is available from NASA'—s Shuttle Radar Topography Mission (SRTM) data (https://lpdaac.usgs.gov/products/srtmgl1v003/). Intermediate data and scripts used to generate the results in this study are available from the corresponding author upon reasonable request.

Author contributions

Chao Yue and Sebastiaan Luyssaert designed the study. Huanhuan Wang conducted the analysis. All three authors contributed to writing and revision of the text.

Competing interests

The authors have the following competing interests: At least one of the (co-)authors is a member of the editorial board of Biogeosciences.

Acknowledgments

This study was supported by the Strategic Priority Research Program of the Chinese Academy of Sciences (grant no. XDB40020000) and by the National Natural Science Foundation of China (grant no. 41971132).

References

Alkama, R. and Cescatti, A.: Biophysical climate impacts of recent changes in global forest cover, Science, 351, 600–604, https://doi.org/10.1126/science.aac8083, 2016.

Bonan, G. B.: Forests and climate change: forcings, feedbacks, and the climate benefits of forests, Science, 320, 1444–1449, https://doi.org/10.1126/science.1155121, 2008.

Bryan, B. A., Gao, L., Ye, Y., Sun, X., Connor, J. D., Crossman, N. D., Stafford-Smith, M., Wu, J., He, C., Yu, D., Liu, Z., Li, A., Huang, Q., Ren, H., Deng, X., Zheng, H., Niu, J., Han, G., and Hou, X.: China’s response to a national land-system sustainability emergency, Nature, 559, 193–204, https://doi.org/10.1038/s41586-018-0280-2, 2018.

Chen, C., Park, T., Wang, X., Piao, S., Xu, B., Chaturvedi, R. K., Fuchs, R., Brovkin, V., Ciais, P., Fensholt, R., Tømmervik, H., Bala, G., Zhu, Z., Nemani, R. R., and Myneni, R. B.: China and India lead in greening of the world through land-use management, Nat Sustain, 2, 122–129, https://doi.org/10.1038/s41893-019-0220-7, 2019.

Chen, J., Chen, J., Liao, A., Cao, X., Chen, L., Chen, X., He, C., Han, G., Peng, S., and Lu, M.: Global land cover mapping at 30 m resolution: A POK-based operational approach, 103, 7–27, https://doi.org/10.1016/j.isprsjprs.2014.09.002, 2015.

Chen, L. and Dirmeyer, P. A.: Adapting observationally based metrics of biogeophysical feedbacks from land cover/land use change to climate modeling, Environ. Res. Lett., 11, 034002, https://doi.org/10.1088/1748-9326/11/3/034002, 2016.

Chen, H., Zeng, Z., Wu, J., Peng, L., Lakshmi, V., Yang, H., and Liu, J.: Large Uncertainty on Forest Area Change in the Early 21st Century among Widely Used Global Land Cover Datasets, Remote Sensing, 12, 3502, https://doi.org/10.3390/rs12213502, 2020.

Cs, M., G, S., and Y, Z.: Afforestation and forests at the dryland edges: lessons learned and future outlooks. In: Chen J, Wan S, Henebry G, Qi J, Gutman G, Sun G, Kappas M (szerk.) Dryland East Asia: Land dynamics amid social and climate change. HEP Publishers, Beijing & Walter de Gruyter and Co. Berlin, 2013, 245–264, https://doi.org/10.13140/RG.2.1.4325.4487, 2013.

Duveiller, G., Hooker, J., and Cescatti, A.: The mark of vegetation change on Earth’s surface energy balance, Nat Commun, 9, 679, https://doi.org/10.1038/s41467-017-02810-8, 2018.

Duveiller, G., Caporaso, L., Abad-Viñas, R., Perugini, L., Grassi, G., Arneth, A., and Cescatti, A.: Local biophysical effects of land use and land cover change: towards an assessment tool for policy makers, Land Use Policy, 91, 104382, https://doi.org/10.1016/j.landusepol.2019.104382, 2020.

Fang, J., Guo, Z., Hu, H., Kato, T., Muraoka, H., and Son, Y.: Forest biomass carbon sinks in East Asia, with special reference to the relative contributions of forest expansion and forest growth, Global Change Biology, 20, 2019–2030, https://doi.org/10.1111/gcb.12512, 2014.

Ge, J., Guo, W., Pitman, A. J., De Kauwe, M. G., Chen, X., and Fu, C.: The Nonradiative Effect Dominates Local Surface Temperature Change Caused by Afforestation in China, 32, 4445–4471, https://doi.org/10.1175/JCLI-D-18-0772.1, 2019.

Hansen, M. C., Potapov, P. V., Moore, R., Hancher, M., Turubanova, S. A., Tyukavina, A., Thau, D., Stehman, S. V., Goetz, S. J., and Loveland, T. R.: High-resolution global maps of 21st-century forest cover change, 342, 850–853, https://doi.org/10.1126/science.1244693, 2013.

Huang, L., Zhai, J., Liu, J., and Sun, C.: The moderating or amplifying biophysical effects of afforestation on CO2-induced cooling depend on the local background climate regimes in China, Agricultural and Forest Meteorology, 260–261, 193–203, https://doi.org/10.1016/j.agrformet.2018.05.020, 2018.

Jia, G., Shevliakova, E., Artaxo, P., Noblet-Ducoudré, N. D., Houghton, R., Anderegg, W., Bastos, A., Bernsten, T. K., Cai, P., Calvin, K., Klein, C. D., Humpenöder, F., Kanter, D., McDermid, S., Peñuelas, J., Pradhan, P., Quesada, B., Roe, S., Bernier, P., Espinoza, J. C., Semenov, S., and Xu, X.: Climate Change and Land: an IPCC Special Report on Climate Change, Desertification, Land Degradation, Sustainable Land Management, Food Security, and Greenhouse Gas Fluxes in Terrestrial Ecosystems. 2019.

Juang, J.-Y., Katul, G., Siqueira, M., Stoy, P., and Novick, K.: Separating the effects of albedo from eco-physiological changes on surface temperature along a successional chronosequence in the southeastern United States, Geophys. Res. Lett., 34, 21, https://doi.org/10.1029/2007GL031296, 2007.

Kato, S., Rose, F. G., Rutan, D. A., Thorsen, T. J., Loeb, N. G., Doelling, D. R., Huang, X., Smith, W. L., Su, W., and Ham, S.-H.: Surface Irradiances of Edition 4.0 Clouds and the Earth's Radiant Energy System (CERES) Energy Balanced and Filled (EBAF) Data Product, 31, 4501–4527, https://doi.org/10.1175/JCLI-D-17-0523.1, 2018.

Lee, X., Goulden, M. L., Hollinger, D. Y., Barr, A., Black, T. A., Bohrer, G., Bracho, R., Drake, B., Goldstein, A., Gu, L., Katul, G., Kolb, T., Law, B. E., Margolis, H., Meyers, T., Monson, R., Munger, W., Oren, R., Paw U, K. T., Richardson, A. D., Schmid, H. P., Staebler, R., Wofsy, S., and Zhao, L.: Observed increase in local cooling effect of deforestation at higher latitudes, Nature, 479, 384–387, https://doi.org/10.1038/nature10588, 2011.

Lee, S. and Lee, D. K.: What is the proper way to apply the multiple comparison test?, Korean J Anesthesiol, 71, 353–360, https://doi.org/10.4097/kja.d.18.00242, 2018.

Li, Y., Zhao, M., Motesharrei, S., Mu, Q., Kalnay, E., and Li, S.: Local cooling and warming effects of forests based on satellite observations, Nature Communications~~Nat. Clim. Chang.~~, 6, 6603, https://doi.org/10.1038/ncomms7603, 2015.

Li, Y., Zhao, M., Mildrexler, D. J., Motesharrei, S., Mu, Q., Kalnay, E., Zhao, F., Li, S., and Wang, K.: Potential and Actual impacts of deforestation and afforestation on land surface temperature: IMPACTS OF FOREST CHANGE ON TEMPERATURE, J. Geophys. Res. Atmos., 121, 14,372-14,386, https://doi.org/10.1002/2016JD024969, 2016a.

Li, Y., De Noblet-Ducoudré, N., Davin, E. L., Motesharrei, S., Zeng, N., Li, S., and Kalnay, E.: The role of spatial scale and background climate in the latitudinal temperature response to deforestation, Earth Syst. Dynam., 7, 167–181, https://doi.org/10.5194/esd-7-167-

2016, 2016b.

Li, Y., Piao, S., Chen, A., Ciais, P., and Li, L. Z. X.: Local and teleconnected temperature effects of afforestation and vegetation greening in China, National Science Review, 7, 897–912, https://doi.org/10.1093/nsr/nwz132, 2020.

Liang, W., Fu, B., Wang, S., Zhang, W., Jin, Z., Feng, X., Yan, J., Liu, Y., and Zhou, S.: Quantification of the ecosystem carrying capacity on China's Loess Plateau, Ecological Indicators, 101, 192–202, https://doi.org/10.1016/j.ecolind.2019.01.020, 2019.

Liu, Y.: China's forest resource dynamics based on allometric scaling relationship between forest area and total stocking volume, Afr. J. Agric. Res., 7, https://doi.org/10.5897/AJAR12.216, 2012.

Liu, Z., Ballantyne, A. P., and Cooper, L. A.: Increases in Land Surface Temperature in Response to Fire in Siberian Boreal Forests and Their Attribution to Biophysical Processes, Geophys. Res. Lett., 45, 6485–6494, https://doi.org/10.1029/2018GL078283, 2018.

Oleson, K., Lawrence, D., Bonan, G., Drewniak, B., Huang, M., Koven, C., Levis, S., Li, F., Riley, W., Subin, Z., Swenson, S., Thornton, P., Bozbiyik, A., Fisher, R., Heald, C., Kluzek, E., Lamarque, J.-F., Lawrence, P., Leung, L., and Yang, Z.-L.: Technical description of version 4.5 of the Community Land Model (CLM), https://doi.org/10.5065/D6RR1W7M, 2013.

Pan, Y., Birdsey, R. A., Fang, J., Houghton, R., Kauppi, P. E., Kurz, W. A., Phillips, O. L., Shvidenko, A., Lewis, S. L., Canadell, J. G., Ciais, P., Jackson, R. B., Pacala, S. W., McGuire, A. D., Piao, S., Rautiainen, A., Sitch, S., and Hayes, D.: A Large and Persistent Carbon Sink in the World's Forests, 333, 988–993, https://doi.org/10.1126/science.1201609, 2011.

Peng, S.-S., Piao, S., Zeng, Z., Ciais, P., Zhou, L., Li, L. Z. X., Myneni, R. B., Yin, Y., and

Zeng, H.: Afforestation in China cools local land surface temperature, Proceedings of the National Academy of Sciences, 111, 2915–2919, https://doi.org/10.1073/pnas.1315126111, 2014.

Pongratz, J., Schwingshackl, C., Bultan, S., Obermeier, W., Havermann, F., and Guo, S.: Land Use Effects on Climate: Current State, Recent Progress, and Emerging Topics, Curr Clim Change Rep, 7, 99–120, https://doi.org/10.1007/s40641-021-00178-y, 2021.

Pitman, A. J., de Noblet-Ducoudré, N., Cruz, F. T., Davin, E. L., Bonan, G. B., Brovkin, V., Claussen, M., Delire, C., Ganzeveld, L., and Gayler, V.: Uncertainties in climate responses to past land cover change: First results from the LUCID intercomparison study, Geophys. Res. Lett., 36, https://doi.org/10.1029/2009GL039076, 2009.

Pitman, A. J., Avila, F. B., Abramowitz, G., Wang, Y. P., Phipps, S. J., and de Noblet-Ducoudré, N.: Importance of background climate in determining impact of land-cover change on regional climate, Nat. Clim. Chang., 1, 472–475, https://doi.org/10.1038/nclimate1294, 2011.

Qi, Y. and Wu, T.: The politics of climate change in China, WIREs Clim Change, 4, 301–313, https://doi.org/10.1002/wcc.221, 2013.

Shen, W., He, J., Huang, C., and Li, M.: Quantifying the Actual Impacts of Forest Cover Change on Surface Temperature in Guangdong, China, Remote Sensing, 12, 2354, https://doi.org/10.3390/rs12152354, 2020.

Sulla-Menashe, D. and Friedl, M. A.: User guide to collection 6 MODIS land cover (MCD12Q1 and MCD12C1) product, 1–18, 2018.

Swann, A. L., Fung, I. Y., and Chiang, J. C.: Mid-latitude afforestation shifts general circulation and tropical precipitation, Proceedings of the National Academy of Sciences, 109, 712–716, https://doi.org/10.1073/pnas.1116706108, 2012.

UC Berkely. Spring 2008 - Stat C141/ Bioeng C141 - Statistics for Bioinformatics

Winckler, J., Reick, C. H., Bright, R. M., and Pongratz, J.: Importance of Surface Roughness for the Local Biogeophysical Effects of Deforestation, J. Geophys. Res. Atmos., 124, 8605–8618, https://doi.org/10.1029/2018JD030127, 2019a.

Winckler, J., Lejeune, Q., Reick, C. H., and Pongratz, J.: Nonlocal Effects Dominate the Global Mean Surface Temperature Response to the Biogeophysical Effects of Deforestation, Geophys. Res. Lett., 46, 745–755, https://doi.org/10.1029/2018GL080211, 2019b.

Windisch, M. G., Davin, E. L., and Seneviratne, S. I.: Prioritizing forestation based on biogeochemical and local biogeophysical impacts, Nat. Clim. Chang., 11, 867–871, https://doi.org/10.1038/s41558-021-01161-z, 2021.

Zeng, Z., Wang, D., Yang, L., Wu, J., Ziegler, A. D., Liu, M., Ciais, P., Searchinger, T. D., Yang, Z.-L., Chen, D., Chen, A., Li, L. Z. X., Piao, S., Taylor, D., Cai, X., Pan, M., Peng, L., Lin, P., Gower, D., Feng, Y., Zheng, C., Guan, K., Lian, X., Wang, T., Wang, L., Jeong, S.-J., Wei, Z., Sheffield, J., Caylor, K., and Wood, E. F.: Deforestation-induced warming over tropical mountain regions regulated by elevation, Nature Geoscience, 14, 23–29, https://doi.org/10.1038/s41561-020-00666-0, 2021.

Zhang, L., Marron, J. S., Shen, H., and Zhu, Z.: Singular Value Decomposition and Its Visualization, Journal of Computational and Graphical Statistics, 16, 833–854, https://doi.org/10.1198/106186007X256080, 2007.

Zhang, Y., Chen, Y., Li, J., and Chen, X.: A Simple Method for Converting 1-km Resolution Daily Clear-Sky LST into Real LST, Remote Sensing, 12, 1641, https://doi.org/10.3390/rs12101641, 2020.

Zhao, K. and Jackson, R. B.: Biophysical forcings of land-use changes from potential forestry activities in North America, Ecological Monographs, 84, 329–353, https://doi.org/10.1890/12-1705.1, 2014.

Ziter, C. D., Pedersen, E. J., Kucharik, C. J., & Turner, M. G. (2019). Scale-dependent interactions between tree canopy cover and impervious surfaces reduce daytime urban heat during summer. Proceedings of the National Academy of Sciences, 116(15), 7575–7580. https://doi.org/10.1073/pnas.1817561116